Fitting circles to data with correlated noise

N. Chernov [a] P. N. Sapirstein [b]

[a] *Department of Mathematics, University of Alabama at Birmingham, Birmingham, AL 35294*

[b] *Department of the History of Art and Archaeology, Cornell University, Ithaca, NY 14853*

Abstract

We study the problem of fitting circles to scattered data. Unlike many other studies, we assume that the noise is (strongly) correlated; we adopt a particular model where correlations decay exponentially with the distance between data points. Our main results are formulas for the maximum likelihood estimates and their covariance matrix. Our study is motivated by (and applied to) arcs collected during archeological field work.

Key words: fitting circles, least squares, maximum likelihood, correlated noise.

1 Introduction

Fitting circles to imperfect (noisy or distorted) images is a common task in pattern recognition (Pei and Horng (1996)), computer vision (Atieg and Watson (2004)), industry (quality control) (Landau (1987)), high energy physics (Chernov and Ososkov (1984); Karimäki (1991)), medical sciences (Biggerstaff (1972)), archeology (DeBoer (1980); Freeman (1977); Haliř and Flusser (1998); Haliř and Menard (1996); Plog (1985); Thom (1955); Whalen (1998)), robotics (Zhang et al. (2006)), and many other areas of human practice.

Theoretical and statistical analysis of the problem has been done by Chan (1965); Berman and Culpin (1986); Berman (1989); Thomas and Chan (1989); Chan and Thomas (1995); Kanatani (1998); Nievergelt (2002); Yin and Wang (2004); Chan et al. (2005); Chernov and Lesort (2005); Zelniker and Clarkson (2006); and others. In all these works the observed points were assumed to have independent normal distribution (specified below). Practical algorithms for fitting circles to data were proposed in the above papers, and also by Landau (1987); Späth (1996), see a survey by Chernov and Lesort (2005).

Our paper is motivated by a common archaeological problem of estimating the diameter of a potsherd from a field expedition. The original diameter at specific point along the profile of a broken pot – such as the outer rim or base – is restored by fitting a circle to a sherd.

Typically, archaeologists refer to a diameter chart to estimate the diameter of sherds, but the accuracy of this method is poor; see DeBoer (1980); Plog (1985); Whalen (1998). When tested, this chart-fitting technique has been found to produce a standard error of 5% to 10% of the estimate; see Hagstrum and Hildebrand (1983), (Pot and de Groot, 1989, pp. 34–36), and (Whalen, 1998, Table 1). Moreover, individuals do not always read the charts consistently. Even with relatively well-preserved sherds, the average readings from different examiners during fieldwork have been documented to vary by as much as 5% to 10% of the estimate; see DeBoer (1980), (Plog et al., 1978, pp. 413–415), and Plog (1985). Thus, the methods presently employed in most archaeological fieldwork limit the many analytical techniques which rely on diameter estimates of potsherds. We develop a new mathematical model and practical algorithms that overcome the limitations of the techniques currently in use.

In general, the ideal contour which one fits to observed data is defined by an equation

$$P(x, y; \mathbf{\Theta}) = 0, \tag{1}$$

where P is a polynomial in x and y and $\mathbf{\Theta} = [\theta_1, \dots, \theta_k]^T$ is a vector of coefficients (unknown parameters) to be estimated. For example, a circle is defined by

$$(x - a)^2 + (y - b)^2 - R^2 = 0, \tag{2}$$

hence $\mathbf{\Theta} = (a, b, R)$ is a 3D parameter vector. This work focuses on circles, but our methods can be extended to other curves as well.

The imperfect image is represented by a set of points $(x_1, y_1), \dots, (x_n, y_n)$ obtained by scanning or otherwise digitizing the observed curve. One then finds the curve satisfying (1) that provides the best fit to these points, usually by minimizing the sum of squares of the distances to the data points

$$\mathcal{F}_0(\mathbf{\Theta}) = \sum_{i=1}^{n} d_i^2, \tag{3}$$

where d_i denotes the geometric (orthogonal) distance from (x_i, y_i) to the curve (1). This method is known as the *geometric fit*, or *least squares fit* (LSF).

In theoretical studies, one usually adopts a statistical model where each (x_i, y_i) is a noisy observation of some *true (or idealized) point* (x_i^*, y_i^*), i.e.

$$x_i = x_i^* + \delta_i, \qquad y_i = y_i^* + \varepsilon_i, \qquad i = 1, \dots, n, \tag{4}$$

where $(\delta_1, \varepsilon_1), \dots, (\delta_n, \varepsilon_n)$ are small random vectors (disturbances). The true

points (x_i^*, y_i^*) are supposed to lie on a 'true (or idealized) curve', i.e. satisfy

$$P(x_i^*, y_i^*; \mathbf{\Theta}^*) = 0, \qquad i = 1, \ldots, n, \tag{5}$$

where $\mathbf{\Theta}^*$ is the vector of true (unknown) parameters.

In virtually all studies the disturbances $(\delta_1, \varepsilon_1), \ldots, (\delta_n, \varepsilon_n)$ are assumed to be independent random vectors with zero mean. It is also often assumed that each $(\delta_i, \varepsilon_i)$ is a normal (Gaussian) vector with some covariance matrix $\mathbf{C}_i$. The simplest choice is $\mathbf{C}_i = \sigma^2\mathbf{I}$, in which case all errors ε_i and δ_i are normal random variables with zero mean and a common variance σ^2. In that case the geometric fit minimizing (3) is mathematically equivalent to the maximum likelihood estimation (MLE); see e.g. Chan (1965).

In this paper we challenge and modify the assumption that disturbances are independent. That assumption may be appropriate when the noise is due to purely technical reasons, such as imperfect scanning, imprecise recording, etc. There are, however, different causes of disturbances which make them strongly dependent.

For example, a manufactured circular object like a disk or pot may in fact have small bumps or cavities in its profile. Such defects are common on ancient potsherds coated with burial accretions and damaged by use, discard, and burial processes. Moreover, some objects that appear generally round may in reality be slightly distorted. A wheel-thrown pot will always exhibit some warping at various places in its walls due to imperfect manufacturing or uneven shrinkage during drying and firing.

In a common situation from high energy physics, the trajectory of an elementary particle in a constant magnetic field must be circular, but the curvature of the particle's track may vary slightly due to inhomogeneities of the magnetic field.

In these cases deviations of data points $(x_1, y_1), \ldots, (x_n, y_n)$ from the ideal circle may occur *in unison*: a long string of nearby points may lie outside the ideal circle, while another string elsewhere along the circumference may lie inside it. Consequently, the disturbances become strongly correlated; more precisely, the correlation is strong between nearby points but weakens between distant points.

Correlations may also be introduced in the process of digitizing. In the archaeological field data presented below, sherd profiles are traced on a sheet of graph paper which is later scanned and transformed into an array of pixels (data points). Profiles may be traced with a pencil directly from the sherd placed on the paper, but when this is impossible the profile is obtained indirectly by means of a profile gauge. In both situations the point of the pencil

inevitably strays slightly from the true shape of the object, deflecting a string of points inside or outside the true circle.

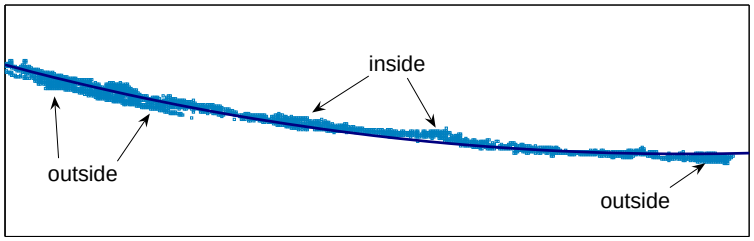

Fig. 1. A magnified view of a line drawn by pencil along the edge of a sherd (grey pixels) and the best-fitting circle (dark thin arc). Arrows point out places where pixels stray mostly inside the arc or mostly outside the arc.

Fig. 1 shows part of the digitized pencil line from an archaeological field study and its best-fitting circle. The pencil line sometimes strays inside the fitted circle and sometimes outside it, creating fairly long deflections.

Despite all the high potential for correlations between disturbances in arcs from various applications, there are no commonly adopted statistical models of this effect. The topic remains virtually unexplored.

We will show that in the presence of correlations the least squares fit remains adequate, i.e. the best point estimates of the parameters of the fitted curve are the same with or without correlations. However, correlations between disturbances strongly affect standard deviations of the estimates – and, hence, the corresponding confidence intervals.

A model that takes correlations into account has potentially broad applications for archaeological research. Having an estimate of the confidence interval of a fitted diameter allows a variety of improvements to classification systems for individual potsherds as well as more sophisticated tests of excavated assemblages.

We present a statistical model that incorporates strong correlations between data points. The strength of correlations is controlled by one parameter which can easily be estimated from the data. We also derive the respective maximum likelihood estimates (MLE) of the model parameters and obtain formulas for their covariance matrix. Our formulas happen to be surprisingly simple and easy to implement. We illustrate their application with simulated and archaeological data.

2 General correlation model

Each disturbance vector $(\delta_i, \varepsilon_i)$, $i = 1, \ldots, n$, has a normal (radial) component d_i and a tangential component e_i. The important one is d_i, which represents the (signed) distance from the data point (x_i, y_i) to the curve (to the leading order of magnitude). In Fig. 2 the tangential component e_i is practically irrelevant.

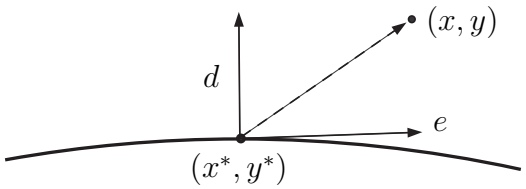

Fig. 2. A true (idealized) point (x^*, y^*) and the corresponding observed point (x, y); the radial component d and the tangential component e of the disturbance vector $(x - x^*, y - y^*)$.

In fact some statisticians assume that the disturbance vector $(\delta_i, \varepsilon_i)$ is always orthogonal to the true curve, i.e. the noise occurs only in the radial direction, which eliminates tangential displacements altogether. Berman and Culpin (1986) call this a *radial model*, and we adopt it here.

Now for each $i = 1, \ldots, n$ we denote by

$$d_i = d_i(a, b, R) = \sqrt{(x_i - a)^2 + (y_i - b)^2} - R$$

the (signed) distances from the data point (x_i, y_i) to the circle with parameters (a, b, R). We assume that $E(d_i) = 0$ and denote by

$$\mathbf{V} = E(\mathbf{D}\mathbf{D}^T)$$

the covariance matrix of the vector $\mathbf{D} = (d_1, \ldots, d_n)^T$; the components of $\mathbf{V}$ are $v_{ij} = E(d_i d_j)$.

Assume for a moment that $\mathbf{V}$ is known. The likelihood function is

$$f(d_1, \ldots, d_n) = \frac{1}{[(2\pi)^n \det \mathbf{V}]^{1/2}} \exp\Big[-\frac{1}{2}\,\mathbf{D}^T\mathbf{V}^{-1}\mathbf{D}\Big],$$

so the maximum likelihood estimates of a, b, R are obtained by minimizing

$$\mathcal{F}_1(a, b, R) = \mathbf{D}^T\mathbf{V}^{-1}\mathbf{D}. \tag{6}$$

In the standard model with no correlations, we have $\mathbf{V} = \sigma^2\mathbf{I}$, and then minimizing (6) is equivalent to minimizing (3); this brings us back to the least squares fit.

Next we compute the covariance matrix of the maximum likelihood estimates. By using standard Taylor series approximation

$$\begin{aligned} d_i &= \sqrt{(x_i-a)^2+(y_i-b)^2} - R \\ &= \sqrt{(x_i-a^*-\delta a)^2+(y_i-b^*-\delta b)^2} - R^* - \delta R \\ &\approx \bar{d}_i - u_i\,\delta a - v_i\,\delta b - \delta R, \end{aligned} \tag{7}$$

where $\bar{d}_i = \sqrt{(x_i-a^*)^2+(y_i-b^*)^2} - R^*$ designates the distance to the true circle, and we denote

$$u_i = (x_i^*-a^*)/R^* \quad \text{and} \quad v_i = (y_i^*-b^*)/R^*.$$

Observe that $u_i = \cos\varphi_i$ and $v_i = \sin\varphi_i$, where φ_i is the angular coordinate of the true point (x_i^*, y_i^*) on the true circle, as is clear from the following:

$$x_i^* = a^* + R^*\cos\varphi_i, \qquad y_i^* = b^* + R^*\sin\varphi_i. \tag{8}$$

In matrix form, (7) can be written as

$$\mathbf{D} = \bar{\mathbf{D}} - \mathbf{U}\,\delta\boldsymbol{\Theta},$$

where

$$\mathbf{U} = \begin{bmatrix} u_1 & v_1 & 1 \\ \vdots & \vdots & \vdots \\ u_n & v_n & 1 \end{bmatrix} \quad \text{and} \quad \delta\boldsymbol{\Theta} = \begin{bmatrix} \delta a \\ \delta b \\ \delta R \end{bmatrix}.$$

Now (6) takes form

$$\mathcal{F}_1 = \bar{\mathbf{D}}^T\mathbf{V}^{-1}\bar{\mathbf{D}} - 2\,\delta\boldsymbol{\Theta}^T\,\mathbf{U}^T\mathbf{V}^{-1}\bar{\mathbf{D}} + \delta\boldsymbol{\Theta}^T\,\mathbf{U}^T\mathbf{V}^{-1}\mathbf{U}\,\delta\boldsymbol{\Theta}$$

and its minimum is attained at

$$\delta\boldsymbol{\Theta} = (\mathbf{U}^T\mathbf{V}^{-1}\mathbf{U})^{-1}\mathbf{U}^T\mathbf{V}^{-1}\bar{\mathbf{D}}$$

Since $E(\bar{\mathbf{D}}) = 0$, it follows that $E(\delta\boldsymbol{\Theta}) = 0$ so that our estimates are unbiased (to the leading order). Their covariance matrix is

$$\begin{aligned} \mathrm{Cov}(\boldsymbol{\Theta}) &= E(\delta\boldsymbol{\Theta}\,\delta\boldsymbol{\Theta}^T) \\ &= (\mathbf{U}^T\mathbf{V}^{-1}\mathbf{U})^{-1}\mathbf{U}^T\mathbf{V}^{-1}E(\bar{\mathbf{D}}\bar{\mathbf{D}}^T)\mathbf{V}^{-1}\mathbf{U}(\mathbf{U}^T\mathbf{V}^{-1}\mathbf{U})^{-1} \\ &= (\mathbf{U}^T\mathbf{V}^{-1}\mathbf{U})^{-1}, \end{aligned} \tag{9}$$

because $E(\bar{\mathbf{D}}\bar{\mathbf{D}}^T) = \mathbf{V}$. Again, in the standard model with no correlations we have $\mathbf{V} = \sigma^2\mathbf{I}$, and we recover the well-known formula, see e.g. Chernov and Lesort (2004); Kanatani (1998):

$$\mathrm{Cov}(\boldsymbol{\Theta}) = \sigma^2(\mathbf{U}^T\mathbf{U})^{-1}. \tag{10}$$

We see that the objective function (6) for computing maximum likelihood estimates and the corresponding covariance matrix formula (9) involve the inverse matrix $\mathbf{V}^{-1}$ of the covariances of disturbances. Our next goal is to adopt a model in which $\mathbf{V}^{-1}$ is tractable.

REMARK. In practice the minimization of (6) may be difficult, depending on the structure of the matrix $\mathbf{V}^{-1}$ (see the next section). Then one may still use the ordinary least squares fit (3). In that case the objective function (3) takes form

$$\mathcal{F}_0 = \bar{\mathbf{D}}^T\bar{\mathbf{D}} - 2\,\delta\boldsymbol{\Theta}^T\,\mathbf{U}^T\bar{\mathbf{D}} + \delta\boldsymbol{\Theta}^T\,\mathbf{U}^T\mathbf{U}\,\delta\boldsymbol{\Theta},$$

its minimum is attained at

$$\delta\boldsymbol{\Theta} = (\mathbf{U}^T\mathbf{U})^{-1}\mathbf{U}^T\bar{\mathbf{D}},$$

and the covariance matrix is now given by

$$\mathrm{Cov}(\boldsymbol{\Theta}) = (\mathbf{U}^T\mathbf{U})^{-1}\mathbf{U}^T\mathbf{V}\mathbf{U}(\mathbf{U}^T\mathbf{U})^{-1}. \tag{11}$$

3 Simple structure of correlations

A specific assumption about the covariance matrix $\mathbf{V}$ makes practical calculations feasible.

First we assume that the array of the data points is ordered along the circumference; i.e. their angular coordinates φ_i, see (8), are sorted either in ascending or descending order. This is easily performed after fitting a circle to unsorted data. Now the value $|i-j|$ roughly represents the distance between the points (x_i^*, y_i^*) and (x_j^*, y_j^*).

Because the correlations must be stronger between nearby points and weaker between distant points, we assume that they decay exponentially with distance; i.e. the components of $\mathbf{V}$ satisfy

$$v_{ij} = \sigma^2\rho^{|i-j|} \tag{12}$$

for some $\rho < 1$. Here σ^2 is a common variance of every deviation d_i and $\rho^{|i-j|}$ is the correlation between d_i and d_j. The parameter ρ controls the strength of correlations: they are strong for ρ close to 1, weak for ρ near 0, and vanish completely if $\rho = 0$, in which case (12) becomes $v_{ii} = \sigma^2$ and $v_{ij} = 0$ for $i \neq j$.

REMARK. We can also justify our assumption (12) theoretically as follows. Suppose the noise vectors $(\delta_i, \varepsilon_i)$ are dependent and form a Markov chain, i.e. each observed point (x_i, y_i) depends on the previous one (x_{i-1}, y_{i-1}) but not

on the earlier ones (x_{i-m}, y_{i-m}), $m \geq 2$. Then the covariance matrix satisfies (12), see Feller (1971), page 97. Our Markovness assumption is natural when points are drawn by a pencil, as the pencil tip moves continuously from one data point to the next.

Now the inverse of $\mathbf{V}$ specified by (12) is a tridiagonal matrix:

$$\mathbf{V}^{-1} = \frac{\sigma^{-2}}{1-\rho^2} \begin{bmatrix} 1 & -\rho & 0 & 0 & \dots & 0 \\ -\rho & 1+\rho^2 & -\rho & 0 & & 0 \\ 0 & -\rho & 1+\rho^2 & -\rho & \ddots & 0 \\ 0 & 0 & -\rho & 1+\rho^2 & & 0 \\ \vdots & & \ddots & & \ddots & \vdots \\ 0 & \dots & 0 & -\rho & 1+\rho^2 & -\rho \\ 0 & \dots & 0 & 0 & -\rho & 1 \end{bmatrix}.$$

Assume for a moment that ρ is known. Then the minimization of (6), which produces the maximum likelihood estimates, is achieved by minimizing

$$\mathcal{F}_2 = \sum_{i=1}^{n} d_i^2 - \tfrac{2\rho}{1+\rho^2} \sum_{i=1}^{n-1} d_i d_{i+1} \tag{13}$$

(we somewhat simplified the actual expression by modifying it near the ends, i.e. at $i = 1$ and $i = n$). The first sum in (13) is the classical objective function (3), while the second sum represents the correction due to correlations. Note that $\frac{2\rho}{1+\rho^2} < 1$.

The correction term in (13) essentially reduces the contribution of neighboring pairs for which $d_i d_{i+1} > 0$ (i.e. both points lie on one side of the fitted circle) and amplifies the contribution of pairs for which $d_i d_{i+1} < 0$ (points lie on the opposite sides of the fitted circle). In other words, the correction term in (13) suppresses the influence of strings of consecutive points lying on one side of the fitted circle. These strings are likely to be caused by strong correlations and thus do not represent the actual location of the true circle.

In practice, however, the second sum in (13) is unlikely to dramatically change the fitted circle. On the data samples collected during archaeological field work, the differences between the two fits (3) and (13) are negligible. Below we prove that both fits have the same accuracy (the same covariance matrix), to the leading order.

Next we turn to the calculation of the covariance matrix (9). First we derive a simplified formula for the matrix $\sigma^2 \mathbf{U}^T \mathbf{V}^{-1} \mathbf{U}$. The bottom right component

of this matrix is approximately $(1-\rho)^2/(1-\rho^2) = (1-\rho)/(1+\rho)$. The top left component is approximately

$$\frac{1}{1-\rho^2}\sum_i \big[(1+\rho^2)u_i^2 - 2\rho u_i u_{i+1}\big]$$

(here we again somewhat simplified the actual expression near the ends, i.e. at $i=0$ and $i=n$). Now as the points i and $i+1$ are adjacent, we clearly have $u_i \approx u_{i+1}$, so we can safely approximate the above expression by

$$\frac{1+\rho^2-2\rho}{1-\rho^2}\sum_i u_i^2 = \frac{1-\rho}{1+\rho}\sum_i u_i^2.$$

Repeating this procedure for each component of the matrix $\mathbf{U}^T\mathbf{V}^{-1}\mathbf{U}$ we arrive at

$$\sigma^2\,\mathbf{U}^T\mathbf{V}^{-1}\mathbf{U} \approx \tfrac{1-\rho}{1+\rho}\,\mathbf{U}^T\mathbf{U}. \tag{14}$$

As a result,

$$\mathrm{Cov}(\mathbf{\Theta}) \approx \tfrac{1+\rho}{1-\rho}\,\sigma^2(\mathbf{U}^T\mathbf{U})^{-1} = \tfrac{1+\rho}{1-\rho}\,\mathrm{Cov}_0(\mathbf{\Theta}), \tag{15}$$

where $\mathrm{Cov}_0(\mathbf{\Theta})$ is the covariance matrix in the absence of correlations given by (10). Hence the presence of correlations magnify the covariance matrix by a factor of $(1+\rho)/(1-\rho)$. When correlations are not weak (i.e. ρ is not near 0), this factor is significant and cannot be ignored.

Remark. If one uses the least squares estimation minimizing (3), then the covariance matrix is given by (11), instead of (9). In that case, since $v_{ij} = \sigma^2\rho^{|i-j|}$ and again $(u_i, v_i) \approx (u_j, v_j)$ for small[1] $|i-j|$, we have

$$\begin{aligned}\mathbf{U}^T\mathbf{V}\mathbf{U} &\approx \sigma^2(1+2\rho+2\rho^2+\cdots)\mathbf{U}^T\mathbf{U}\\ &= \tfrac{1+\rho}{1-\rho}\,\sigma^2\mathbf{U}^T\mathbf{U}.\end{aligned} \tag{16}$$

Combining this with (11) we arrive at the same final formula (15). Thus the accuracy of both methods – the maximum likelihood (6) and the ordinary least squares (3) – is identical, as far as the approximation (15) goes.

4 Estimation of ρ

In order to use the formulas (13) and (15) in practice we need to estimate ρ from data. Here we do just that.

[1] In our tests on archaeological field data (cf. Section 5) we typically observed $n \sim 10,000$ data points along an arc of $\sim 20^o$ and $\rho \sim 0.995$, hence correlations remain significant for $|i-j| \sim 500$, which is roughly equivalent to $|\varphi_i - \varphi_j| \sim 0.01$; thus indeed we have $(u_i, v_i) \approx (u_j, v_j)$.

First, the standard estimate of σ^2 is

$$\text{estimate}(\sigma^2) = \frac{1}{n-3} \sum_{i=1}^{n} d_i^2. \tag{17}$$

Similarly, the estimate of the one-step correlation term would be

$$\text{estimate}(\sigma^2\rho) = \frac{1}{n-4} \sum_{i=1}^{n-1} d_i d_{i+1}.$$

These two formulas may already be combined to estimate ρ, but we can improve the result by including higher-step correlations as well. For the k-step correlation term we have

$$\text{estimate}(\sigma^2\rho^k) = \frac{1}{n-3-k} \sum_{i=1}^{n-k} d_i d_{i+k}. \tag{18}$$

Adding up these estimates gives

$$\text{estimate}\Big(\sigma^2/(1-\rho)\Big) = \sum_{k\ge 0} \frac{1}{n-3-k} \sum_{i=1}^{n-k} d_i d_{i+k}. \tag{19}$$

In practice we should not include terms with large k's for two reasons. First, correlations between distant points become weak, which makes the contribution from large k's negligible overall. Second, while theoretically the correlations remain positive for every $k \ge 1$ (recall that they are assumed to be $\sigma^2\rho^k$), their estimates (18) for large k's may be negative, and in fact this happens in dangerous proportions (see below).

Indeed, fitting a circle by least squares (3) results in the end with (cf. Chernov and Lesort (2005))

$$\sum_i d_i = 0 \tag{20}$$

(recall that d_i are the signed distances, see (7), which are positive for points outside the circle and negative for those inside it). Squaring (20) gives

$$\sum_{i=1}^{n} d_i^2 + 2 \sum_{k\ge 1} \sum_{i=1}^{n-k} d_i d_{i+k} = 0. \tag{21}$$

This shows not only that some k-step estimates given by (18) are negative, but they must be large enough to cancel all positive estimates, in the sense of (21). For this reason the right hand side of (19), with all k's included, is likely to be negative!

Taking all these facts into consideration we propose a practical solution of

increasing k until the right hand side grows, and then stopping, i.e.,

$$\text{estimate}\Big(\sigma^2/(1-\rho)\Big) = \sum_{k=0}^{m} \frac{1}{n-3-k} \sum_{i=1}^{n-k} d_i d_{i+k}, \tag{22}$$

where

$$m+1 = \min\left\{k\colon \sum_{i=1}^{n-k} d_i d_{i+k} < 0\right\}.$$

Lastly one can combine (17) and (22) as follows:

$$\text{estimate}(\rho) = 1 - \frac{\sum_{i=1}^{n} \frac{1}{n-3}\, d_i^2}{\sum_{k=0}^{m} \frac{1}{n-3-k} \sum_{i=1}^{n-k} d_i d_{i+k}}. \tag{23}$$

5 Experimental tests

Simulated data. To test our formulas on simulated data we first need to generate a sequence of random numbers $d_1, d_2, \ldots$ with a normal distribution, zero mean, and covariances satisfying our model assumptions, i.e. $\mathrm{Cov}(d_i, d_{i+k}) = \sigma^2\rho^k$.

This can be done by setting $d_1 = \sigma z_1$ and then computing $d_2, d_3, \ldots$ sequentially by the rule

$$d_n = \rho d_{n-1} + \sigma_0 z_n,$$

where $z_1, z_2, \ldots$ are independent and identically distributed normal random variables with zero mean, unit variance, and $\sigma_0^2 = (1-\rho^2)\sigma^2$. It is easy to see that the sequence obtained this way has all the desired properties; see also Feller (1971), page 97.

Then we can fix a true circle (a^*, b^*, R^*) (in our tests we choose $(0, 0, 1)$) and a monotonic sequence of angular coordinates $\varphi_1, \ldots, \varphi_n$ (we choose $n = 1000$ and angles equally spaced between 0 and $\varphi_{\max}$). We generate a set of data points by

$$x_i = a^* + (R^* + d_i)\cos\varphi_i, \qquad y_i = b^* + (R^* + d_i)\sin\varphi_i.$$

Then we can fit a circle by the least squares (3) or the maximum likelihood (13), which give practically the same results, and estimate ρ by (23) (although in our tests we employed the more efficient Taubin fit; see the remark in the end of Section 2).

In our tests we set $\sigma = 0.01$ (to make average disturbances small compared to the radius $R^* = 1$), we tried $\varphi_{\max} = \pi$ (semi-circle) and $\varphi_{\max} = \pi/2$ (quarter of a circle), and we varied ρ from 0 to 0.95; for each value of ρ we generated 10^6

	mean ± st.dev.	
ρ	180^o arc	90^o arc
0.0	0.020 ± 0.033	0.020 ± 0.033
0.1	0.112 ± 0.046	0.111 ± 0.046
0.2	0.207 ± 0.050	0.208 ± 0.051
0.3	0.304 ± 0.053	0.304 ± 0.053
0.4	0.400 ± 0.053	0.401 ± 0.053
0.5	0.497 ± 0.052	0.497 ± 0.052
0.6	0.593 ± 0.050	0.593 ± 0.049
0.7	0.689 ± 0.045	0.690 ± 0.045
0.8	0.786 ± 0.037	0.786 ± 0.038
0.9	0.882 ± 0.026	0.883 ± 0.026
0.95	0.931 ± 0.018	0.931 ± 0.018

Table 1
Simulated data.

random samples and computed the mean value and standard deviation of the resulting estimates of ρ. The results are recorded in Table 1. It demonstrates that our formula (23) for estimating ρ is quite accurate (though it tends to slightly underestimate ρ for $\rho \geq 0.5$).

Real world data. We tested our approach on digitized arcs from archaeological fieldwork. The arcs are fragments of wheelmade and molded circular architectural terracottas whose original diameters are unknown. Using a profile gauge, the profiles are transferred to graph paper, scanned, and transformed into an array of black and white pixels with a threshold filter. The data points are the x and y coordinates of black pixels measured in centimeters. The arcs usually consist of 5,000 to 20,000 points and subtend angles ranging from 5^o to 270^o. A typical digitized arc is shown on Fig. 3.

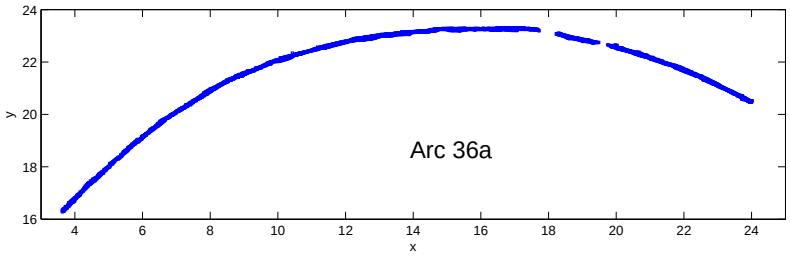

Fig. 3. A typical arc drawn by pencil with a profile gauge from a circular cover tile.

Tests on real data must be done differently, because there is no "theoretical"

value of ρ to which to compare our estimate. Instead, we can estimate the standard deviation of the parameters (a, b, R) empirically. We begin by fitting a circle to the full arc; then we erase a small portion of the arc, refit the circle to the remaining image, and examine the change in the estimated radius R.

This approach is analogous to the standard bootstrapping method, but there is an important difference. We do not just remove 5% or 10% of the sample randomly, as this would not change the overall size or shape of the arc. Instead, we erase 5% of the pencil-drawn arc either from one end or from both ends of the arc. In this way we actually see how the fitted circle depends on the size of the sherd. In effect, we evaluate fluctuations of the radius estimates obtained from various parts of the original round object (the potsherd), and that is what matters in practice.

Table 2 shows the results obtained for several arcs drawn from actual sherds coded by 11a, 22a, etc. Its columns include the estimated radius R (in centimeters); the change in R (denoted by ΔR) after erasing 5% of the arc on each end; the standard deviation of the estimate of the radius, $\sigma_{R,1}$, computed via (15); the 'ordinary' standard deviation (10), $\sigma_{R,0}$, which does not take correlations into account; and the estimate of the correlation parameter ρ.

It is clear that the ordinary formula (10) in most cases grossly underestimates the "empirical" standard deviation of the radius estimate. On the other hand, our formula (15) agrees with the empirical value ΔR, in the sense that the latter falls into its 95% confidence interval

$$|\Delta R| \le 2\sigma_{R,1}$$

in all the tested cases. Our estimate of ρ is always very high indicating the presence of strong correlations in the data.

Lastly, we verified the validity of our assumption (12) by using real data. Figure 4 shows our estimate of $\sigma^2\rho^k$, given by (18), versus $k = 1, \ldots, 1200$, on a logarithmic scale. The linear profile of the plot confirms our assumption that the correlations decay exponentially with k.

6 Conclusions

We propose a new model for fitting geometric curves (and specifically, circles) to images with highly correlated noise. Our model allows us to evaluate correctly the standard deviation of parameter estimators and construct proper confidence intervals for unknown parameters. The classical models which have been adopted in the literature to date assume that noise is uncorrelated. Even

code	object	R (cm)	ΔR (cm)	$\sigma_{R,1}$	$\sigma_{R,0}$	ρ
11a	wheelmade antefix	13.8	0.017	0.075	0.004	0.993
22a	molded cover tile	18.5	0.352	0.206	0.008	0.997
36a	”	13.6	0.126	0.076	0.005	0.992
37a	”	15.7	0.071	0.084	0.002	0.999
55a	”	18.8	0.215	0.365	0.011	0.998
79a	”	18.8	0.160	0.173	0.006	0.997
87a	wheelmade acroterion	38.8	0.163	0.144	0.009	0.992
88a	”	15.6	0.601	0.415	0.035	0.986
90a	”	24.5	0.210	0.605	0.052	0.985
108a	”	66.1	0.602	0.681	0.035	0.995

Table 2
Real data.

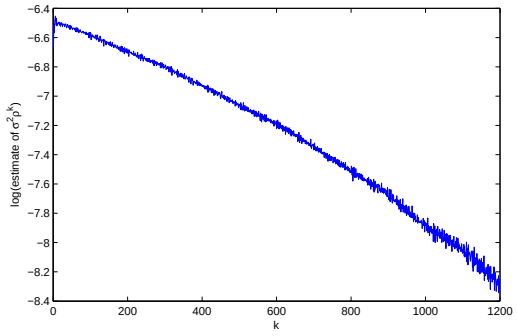

Fig. 4. Our estimate of $\sigma^2\rho^k$, versus k, for the real arc 79a.

though this results in accurate point estimates of unknown parameters, it provides incorrect standard deviations and misleading confidence intervals.

Our results find immediate applications in the archeological research where one estimates the original diameter of potsherds and fragments of other ancient circular objects; adequate confidence intervals for the diameters are essential for identification and classification of such objects.

The fragments analyzed here are from large vessels and wheelmade or molded circular architectural terracottas, which are decorated tiles from sixth-century B.C. roofs. The estimation of the confidence interval improves the ability to distinguish arcs belonging to separate groups. In the case of the rounded tiles, significant variation in the diameter differentiates separate roofing systems from one another.

The method is broadly applicable to the analysis of archaeological ceramics as

well – where classification is a fundamental problem. Standardized measurements that are most descriptive of a vessel type include the full height and the diameters at the rim, base, and maximum; see Roux (2003). With sherds, only the diameter can be determined in most cases. Because the low significance of the fit and inter-examiner bias prevent fine distinctions, however, classifications which rely on arcs fitted to a diameter chart are only able to separate pots of grossly different proportions. More sophisticated tests classify vessels by ratios such as height to rim aperture, and some studies have unwittingly incorporated a significant estimation error by applying these methods to sherds; see (Millet, 1979, P. 37), (Polak, 2000, pp. 74–137), and Poblome (1999).

Other methods for analyzing groups of potsherds from excavations may be improved by our model. A variety of techniques have been developed to estimate vessel volume from the diameter of sherds, yet none has included the confidence interval of the diameter estimate (see, e.g., Blinkhorn (1999); Ericson and de Atley (1976); Hagstrum and Hildebrand (1983); Mounier (1987); Pot and de Groot (1989); Whalen (1998)). One useful measure is the coefficient of variation for standardized pot dimensions, such as rim diameter, which can indicate the intensity of production and the specialization of potters who created a group of vessels (see Ph. J. Arnold (1991), (Ph. J. Arnold, 2000, pp. 111–113), Arnold and Nieves (1992), (Blackman et al., 1993, pp. 71–76) (Frankel, 1988, pp. 42–47), Longacre et al. (1988), (Rice, 1996, pp. 176–182), Roux (2003), Stark (1995), and (Blackman et al., 1993, pp. 38–40)). However, the interpretation of variation in potsherds has been limited by the inherent measurement error of the diameter chart, which obscures the underlying variation in the pot diameters; see Benco (1988); Blackman et al. (1993); Hagstrum (1986). Furthermore, the method proposed here may be adapted to systems for automated classification and reconstruction of vessel types from three-dimensional scanning of sherds; see Gilboa et al. (2004); di Gironimo et al. (2004); Hagstrum and Hildebrand (1990).

Acknowledgments. N.C. is partially supported by NSF grant DMS-0652896. P.S. studied material in the archaeological museums at Aegina (Kolonna), Athens (National Museum), Kerkyra, and Olympia, while supported by the Homer A. and Dorothy B. Thompson Fellowship at the American School of Classical Studies at Athens and the Multi-Country Research Fellowship from the Council of American Overseas Research Centers. The archaeological data will be presented in detail as part of a separate study.

References

Arnold, D. E., Nieves, A. L., 1992. Factors affecting ceramic standardization. In: III, G. J. B., Pool, C. A. (Eds.), Ceramic Production and Distribution: An Integrated Approach. Westview Press, Boulder, pp. 93–113.

Atieg, A., Watson, G. A., 2004. Fitting circular arcs by orthogonal distance regression. Appl. Numer. Anal. Comput. Math., 66–76.

Benco, N. L., 1988. Morphological standardization: An approach to the study of craft specialization. In: Kolb, C. C., Lackey, L. M. (Eds.), A Pot for All Reasons: Ceramic Ecology Revisited. Temple University, Philadelphia, pp. 57–72.

Berman, M., 1989. The asymptotic statistical behaviour of some estimators for a circular structural model. Statist. Prob. Lett., 413–416.

Berman, M., Culpin, D., 1986. The statistical behavior of some least squares estimators of the center and radius of a circle. J. R. Statist. Soc. B, 183–196.

Biggerstaff, R. H., 1972. Three variations in dental arch form estimated by a quadratic equation. J. Dental Res., 1509.

Blackman, M. J., Stein, G. J., Vandiver, P. B., 1993. The standardization hypothesis and ceramic mass production: Technological, compositional, and metric indexes of craft specialization at tell leilan, syria. American Antiquity, 60–80.

Blinkhorn, P., 1999. The trials of being a utensil: Pottery function at the medieval hamlet of west cotton, northamptonshire. Medieval Ceramics, 37–46.

Chan, N. N., 1965. On circular functional relationships. J. R. Statist. Soc. B, 45–56.

Chan, Y. T., Lee, B. H., Thomas, S. M., 2005. Approximate maximum likehood estimation of circle parameters. J. Optim. Applic., 723–733.

Chan, Y. T., Thomas, S. M., 1995. Cramer-Rao lower bounds for estimation of a circular arc center and its radius. Graph. Models Image Proc., 527–532.

Chernov, N., Lesort, C., 2004. Statistical efficiency of curve fitting algorithms. Comp. Stat. Data Anal., 713–728.

Chernov, N., Lesort, C., 2005. Least squares fitting of circles. J. Math. Imag. Vision, 239–251.

Chernov, N. I., Ososkov, G. A., 1984. Effective algorithms for circle fitting. Comp. Phys. Comm., 329–333.

DeBoer, W. R., 1980. Vessel shape from rim sherds: An experiment on the effect of the individual illustrator. J. Field Archaeology, 133–135.

di Gironimo, G., Ferrara, B., Patalano, S., 2004. Definition and construction of parametric archtypes of archaeological artefacts by means of cad technologies. In: der Stadt Wien Referat Ulturelles Erbe Stadarchaeologie Wien, M. (Ed.), Enter the Past: The E-Way into the four Dimensions of Cultural Heritage. Vol. 1227. BAR International Series, Oxford, pp. 86–89.

Ericson, J. E., de Atley, S. P., 1976. Reconstructing ceramic assemblages: An experiment to derive the morphology and capacity of parent vessels from

sherds. American Antiquity, 484–489.
Feller, W., 1971. An Introduction to Probability Theory and Its Applications, Vol. 2, 2nd Edition. John Wiley & Sons.
Frankel, D., 1988. Pottery production in prehistoric bronze age cyprus: Assessing the problem. J. Mediterranean Archaeology, 27–55.
Freeman, P. R., 1977. Note: Thom's survey of the avebury ring. J. Hist. Astronom., 134–136.
Gilboa, A., Karasik, A., Sharon, I., Smilansky, U., 2004. Towards computerized typology and classification of ceramics. J. Archaeological Science, 681–694.
Hagstrum, M. B., 1986. The technology of ceramic production of wanka and inka wares from the yanamarca valley peru. In: Rice, P. M. (Ed.), Ceramic Notes 3. Ceramic Techn. Lab., Florida State Museum, Gainesville, FL, pp. 1–29.
Hagstrum, M. B., Hildebrand, J. A., 1983. Understanding the curvature measurements of potsherds. Pottery Southwest, 3–7.
Hagstrum, M. B., Hildebrand, J. A., 1990. The two-curvature method for reconstructing ceramic morphology. American Antiquity, 388–403.
Haliř, R., Flusser, J., 1998. Numerically stable direct least squares fitting of ellipses. In: Sixth Conf. Cent. Europe Comput. Graph. Vis., WSCG'98, Conf. Proc. Vol. 1. Plzen, Czech Rep., pp. 125–132.
Haliř, R., Menard, C., 1996. Diameter estimation for archaeological pottery using active vision. In: Pinz, A. (Ed.), Proc. 20th Workshop Austrian Assoc. Pattern Recognition (ÖAGM'96). Schloss Seggau, Leibnitz, pp. 251–261.
Kanatani, K., 1998. Cramer-Rao lower bounds for curve fitting. Graph. Mod. Image Process., 93–99.
Karimäki, V., 1991. Effective circle fitting for particle trajectories. Nucl. Instr. Meth. Phys. Res. A, 187–191.
Landau, U. M., 1987. Estimation of a circular arc center and its radius. Computer Vision Graphics Image Proc., 317–326.
Longacre, W. A., Kvamme, K. L., Kobayashi, M., 1988. Southwestern pottery standardization: An ethnoarchaeological view from the Philippines. The Kiva, 101–112.
Millet, M., 1979. An approach to the functional interpretation of pottery. In: Millet, M. (Ed.), Pottery and the Archaeologist. Inst. Archaeology, London, pp. 35–48.
Mounier, R. A., 1987. Estimation of capacity in aboriginal conoidal vessels. J. Middle Atlantic Archaeology, 95–102.
Nievergelt, Y., 2002. A finite algorithm to fit geometrically all midrange lines, circles, planes, spheres, hyperplanes, and hyperspheres. J. Numerische Math., 257–303.
Pei, S.-C., Horng, J.-H., 1996. Optimum approximation of digital planar curves using circular arcs. Pattern Recogn., 383–388.
Ph. J. Arnold, I., 1991. Dimensional standardization and production scale in mesoamerican ceramics. Latin American Antiquity, 363–370.
Ph. J. Arnold, I., 2000. Working without a net: Recent trends in ceramic

ethnoarchaeology. J. Archaeological Research, 105–133.
Plog, S., 1985. Estimating vessel orifice diameters: Measurement methods and measurement error. In: Nelson, B. A. (Ed.), Decoding Prehistoric Ceramics. pp. 243–254.
Plog, S., Plog, F., Wait, W., 1978. Decision making in modern surveys. In: Advances in archaeological method and theory. Vol. 1.
Poblome, J., 1999. Sagalassos red slip ware: Typology and chronology. In: Waelkens, M. (Ed.), Studies in Eastern Mediterranean Archaeology. Vol. 2. Brepols.
Polak, M., 2000. South gaulish terra sigillata with potters' stamps from vechten. In: Rei Cretariae Romanae Fautorum Acta Supplementum. Vol. 9.
Pot, T., de Groot, H. L., 1989. An analysis of rim fragments from 14th-century globular pots excavated in utrecht. Medieval Ceramics, 31–42.
Rice, P. M., 1996. Recent ceramic analysis: 2. composition, production, and theory. J. Archaeological Research, 165–202.
Roux, V., 2003. Ceramic standardization and intensity of production: Quantifying degrees of specialization. American Antiquity, 768–782.
Späth, H., 1996. Least-squares fitting by circles. Computing, 179–185.
Stark, B. L., 1995. Problems in the analysis of standardization and specialization in pottery. In: Mills, B. J., Crown, P. L. (Eds.), Ceramic Production in the American Southwest. Univ. Arizona Press, Tuscon, pp. 231–267.
Thom, A., 1955. A statistical examination of the megalithic sites in britain. J. R. Statist. Soc. A, 275–295.
Thomas, S. M., Chan, Y. T., 1989. A simple approach for the estimation of circular arc center and its radius. Computer Vision Graphics Image Proc., 362–370.
Whalen, M. E., 1998. Ceramic vessel size estimation from sherds: An experiment and a case study. J. Field Archaeology, 219–227.
Yin, S. J., Wang, S. G., 2004. Estimating the parameters of a circle by heteroscedastic regression models. J. Statist. Planning Infer., 439–451.
Zelniker, E., Clarkson, V., 2006. A statistical analysis of the Delogne-Kåsa method for fitting circles. Digital Signal Proc., 498–522.
Zhang, S., Xie, L., Adams, M. D., 2006. Feature extraction for outdoor mobile robot navigation based on a modified gaussnewton optimization approach, 277–287.